N89-12884

FURTHER DEVELOPMENT OF THE DYNAMIC GAS TEMPERATURE MEASUREMENT SYSTEM*

D. L. Elmore, W. W. Robinson, W. B. Watkins
Pratt & Whitney Engineering Division

INTRODUCTION

The objective of this effort was to experimentally verify a dynamic gas temperature measurement system in laboratory experiments. In previous work (Ref. 1) a measurement system was developed for gas turbine combustor exhausts, with special emphasis placed on dynamic response to enable determination of fluctuating components. The measurement probe was demonstrated to have greater than one hour life in a jet engine combustor, and very long (>5 hours) life in an atmospheric burner. Under the current program the measurement and compensation methods were verified by comparing the results obtained by the compensated dynamic sensors with those of a fine-wire resistance thermometer of intrinsically high frequency response. Two signal sources were used: 1) a rotating wheel which alternately directed hot and cold gas streams at the sensors and 2) an atmospheric pressure kerosene/air burner. A commercially available optical fiber thermometer was tested for dynamic response in the burner experiment.

The following sections describe the dynamic gas temperature measurement system verification program. A brief description of the sensor geometry and construction is followed by a discussion of the probe heat transfer analysis and subsequent compensation method. The laboratory experiments are described and experimental results are discussed. Finally, directions for further investigation are given.

PROBE DESCRIPTION

The dynamic temperature probe concept is shown in Figure 1. The probe employs two thermocouples of different wire diameters positioned in close proximity. The thermoelements are large enough in diameter that frequency response above a few Hertz is limited by thermal inertia. When the thermocouples are exposed to the same instantaneous temperature and velocity in the gas stream, the difference in thermal responses will be governed by convective effects (proportional to wire diameter) and conductive effects (proportional to specific heat, thermal conductivity and wire length). Many previous studies (Refs. 2 and 3) used thermoelements of sufficiently large ($\approx$100) length-to-diameter ratio that conduction effects may be neglected, and compensations were based on first-order convective time constants. The present sensor, however, is designed for engine hot-section applications, and the

*Work performed under NASA Contract NAS3-24228

smaller length-to-diameter ratios required for structural adequacy necessitates inclusion of transient conduction effects in the compensation method.

A novel feature of each thermocouple is the beadless, butt-welded thermoelement. The beadless construction allows the sensor to be modelled as a cylinder in crossflow, which simplifies the model considerably. ISA type B (Pt/6Rh - Pt/30Rh) thermocouples were used for the burner tests and type K (chromel-alumel) thermocouples were used for the rotating wheel tests.

PROBE THERMAL ANALYSIS AND COMPENSATION METHOD

The energy conservation equation describing convective and conductive heat transfer to the thermocouples is

$$\frac{dTw}{dt} = \frac{4hg}{\rho wCpwd} (Tg - Tw) + \alpha \frac{d^2Tw}{dx^2} \qquad (1)$$

The thermoelement and support wires were modelled with the nodal breakup shown in Figure 2, and equation (1) is implemented in this model in finite difference form to describe the temperature versus time history of the wire. Material properties for the two t/c legs are averaged in these calculations. To determine the thermocouple response to a given gas stream frequency component, a sinusoidal temperature variation a(t) is used as a boundary condition on the nodes exposed to the gas stream, and several cycles of gas stream temperature are iterated. The true dynamic response of the wire is obtained when peak response amplitudes change less than 0.1% from one-half-cycle to the next.

Comparisons between parametric modelling and experimental data are required in the compensation scheme to determine an in situ value of hg and the resulting compensation spectrum. This method is described as follows. Let the calculated thermocouple and gas stream temperature dynamic amplitudes be denoted by θ_i (f) and a(f), respectively, where i = 1 for the smaller thermocouple and i = 2 for the larger thermocouple. Gas stream signal a(t) is used as a boundary condition for nodes 0-9 and wire temperatures θ_i (t) are calculated at discrete frequencies f_n, over a practical frequency bandwidth (usually 4 to 30 Hz). At each frequency f_n signal amplitude ratio is determined:

$$\theta_i(f_n)/a(f_n) \qquad (2)$$

Note that $\theta_i(f_n)/a(f_n)$ forms a portion of the linear compensation spectrum in the practical bandwidth; this spectrum may be extended to cover the bandwidth of interest. Calculations are repeated for several values of the aerodynamic parameter (Figure 3a)

$$\Gamma = \frac{0.48KgPr^{1/3}\, ug^{1/2}}{\left(\frac{\mu g}{\rho g}\right)^{\frac{1}{2}} \rho w\, Cpw} \qquad (3)$$

which provides aerodynamic scaling between the two different diameter thermocouples (Ref. 1). Note that Γ is proportional to an Hilpert equation (Ref. 4) form of heat transfer coefficient h_g for a cylinder in crossflow:

$$hg = \frac{\rho_w C_{pw}}{d^{\frac{1}{2}}} \quad \Gamma = \frac{0.48 Kg}{d} Pr^{1/3} Re^{1/2} \tag{4}$$

Variation of Γ, therefore, corresponds to a variation in h_g. At constant values of Γ the ratio of the small and large diameter thermocouple responses at given frequencies yields a calculated transfer function $H_c(f_n)$ (Figure 3b).

$$Hc(f_n) = \theta_2(f_n)/\theta_1(f_n) \tag{5}$$

The experimental portion of the compensation method includes recording of the two-wire probe signals, digitizing and converting to temperature using appropriate calibration curves. Temperature versus time waveforms $\theta_i, E(t)$ are Fourier transformed to yield $\theta_i, E(f)$ and division of θ_2 by θ_1 yields an experimental transfer function $H_E(f)$. Experimental and theoretical transfer functions are compared; where the two match at the discrete frequencies in the practical frequency bandwidth, experimental Γ's are then averaged, the calculated $\theta_2(f)/\theta_1(f)$ associated with the average Γ is identified, thereby identifying the calculated $\theta_1(f)/a(f)$, the compensation spectrum gain, and $\eta(f)$, the compensation spectrum phase, for the smaller thermocouple. The calculated compensation spectrum is used over the bandwidth of interest (0-1 KHz). The compensated gas stream temperature spectrum is calculated by dividing the experimentally-measured frequency spectrum by the calculated thermocouple compensation spectrum.

$$a(f) = \theta_{i,E}(f)/(\theta_i(f)/a(f))_c \tag{6}$$

These concepts have been reduced to practice in dynamic temperature sensor compensation software. Fortran coding is used and the program is operational on IBM computers with execution time of about 4 minutes per case.

EXPERIMENT

The rotating wheel experiment is shown in Figure 4. A drive assembly consisting of electric motor and shaft was used to rotate a wheel plate which had 8 holes on a 20.32 cm (8 inch) bolt circle diameter. Heated and ambient temperature air was supplied to two tubes mounted close together on one side of the rotating wheel and in-line with the holes' bolt circle diameter. As the wheel rotated the holes passed the two air supply tubes and allowed hot and cold air pulses to flow. A bifurcated manifold was placed on the opposite side of the rotating wheel in-line with the supply tubes to collect the hot (568K(563F)) and cold (289K(60F)) pulses and feed them into a transition section which became a single circular tube. Hot and cold air pulses were thereby delivered to the sensors mounted immediately downstream of the single circular tube. The wheel was rotated to produce a 250 Hz narrowband signal. Chromel-alumel thermocouples were used in the dynamic temperature sensor, and an analog-compensated 6.4μm (.00025 inch) diameter fine wire resistance thermometer was used as reference sensor.

An atmospheric pressure combustor with flowfield containing large amplitude (several hundred degrees) temperature fluctuations was used as source in the second experiment (Figure 5). An 1159K (1626F) mean temperature test point compared dynamic temperature sensors, a fine wire (12.7μm(.0005 in.) diameter) resistance thermometer and compensated optical fiber thermometer responses in the 0-1 KHZ bandwidth. An 1655K (2519F) mean temperature point

compared dynamic temperature sensor and optical fiber thermometer responses in the same bandwidth. ISA type B thermocouples were used in the dynamic temperature sensor.

RESULTS

A 20 Hz rotating wheel test point was used to derive the Γ for the 250 Hz test point compensation. Compensated 6.4μm (.00025 inch) resistance thermometer and 76μm (.003 inch) thermocouple spectra are shown in Figure 6. Compensated time-domain waveshapes are compared in Figure 7. The 76μm thermocouple has been compensated approximately 28db at the fundamental frequency; the resistance thermometer, however, required 0.9db of compensation due to its inherently higher response.

Figure 8 compares compensated 76μm (3 mil) and 127μm (5 mil) thermocouples and 12.7μm (.0005 mil) resistance thermometer spectra for the atmospheric burner 1159K (1626F) test point. The compensated thermocouples differ by 10% or less over the 0-1 KHz bandwidth, whereas the 12.7μm resistance thermometer is between 37 and 56% lower than the 127μm thermocouple. The amplitude spectrum of the resistance thermometer is shown in Figure 9. Note that a difference of 56% at 1 KHz between the compensated 127μm t/c and 12.7μm resistance thermometer represents about 1.5K$\sqrt{\text{Hz}}$.

Figure 10 is the transfer function between the uncompensated optical fiber thermometer and the compensated 76μm thermocouple for the 1159K (1626F) test point. Figure 11 shows the percentage difference of line amplitudes between the compensated optical fiber thermometer and compensated 76μm (3 mil) thermocouple. Qualitatively similar results were obtained in a second burner test at 1655K (2519F) as shown in Figures 12 and 13.

CONCLUDING REMARKS

The dynamic gas temperature measurement system offers measurement capabilities previously unavailable for gas turbine engines. Structural adequacy of the probes demonstrated in previous work is now more meaningful in combination with measurement fidelity verification. The method can potentially be adapted to transient engine acceleration combustor exit temperature measurements, associated blade and vane cooling flow temperature measurements during transients, as well as used for measurement of steady-state engine dynamic gas temperature signals.

Directions for further work in this measurement technique include fine-tuning and optimization of the basic method as well as extending the work to investigate some fundamental aspects of heat transfer.

1. Measurement uncertainty contribution, both precision and bias, should be determined for each source in the experiment and compensation method, including the fine-wire thermometer standard. The need is to optimize thermoelement diameter ratio and frequency range for determining Γ, and to improve the experimental setup and other factors to minimize uncertainty in the compensated gas stream measurement. Such an uncertainty analysis would involve propagation of uncertainties for

time-dependent quantities, and would require combining uncertainties in both time and frequency domains.

2. The finite-difference model should be extended to include material properties for both halves of the thermoelement. Use of average properties simplifies the model with compromise to uncertainty in the compensation method. The average properties versus individual properties change would determine the corresponding measurement uncertainty contribution, and allow cost versus complexity trade-offs to be made for the compensation scheme.

3. The variation of Γ with frequency should be investigated. The Γ values used in this work were averaged over the practical working bandwidth. Investigation of frequency dependent Γ effects were beyond the scope of this work.

4. Values of hg implicit in Γ should be determined explicitly according to equation (4). The measurement technique developed here offers a novel possibility for measuring hg for a cylinder in crossflow in a combustion stream.

LIST OF SYMBOLS

a = gas stream temperature amplitude at frequency f
Cp = heat capacity
d = thermocouple element diameter
D = thermocouple support wire diameter
f = frequency
$H(f)$ = transfer function
h = convective heat transfer coefficient
K = thermal conductivity
M = Mach number
P = gas pressure
Pr = Prandtl number = $\frac{Cp\mu}{K}$
Re = Reynolds number
T = Temperature
t = time
u = velocity
x = wire length coordinate
α = thermal diffusivity = $\frac{K}{\rho Cp}$
Γ = aerodynamic parameter defined in Equation (3)
μ = viscosity
η = phase shift of thermocouple response with respect to gas temperature at frequency f
ρ = density
θ = thermocouple response

Subscripts

C = calculated
E = experimental
i = 1, 2 denoting smaller and larger thermocouples, respectively
n = frequency index
T = theoretical; total gas properties
w = wire
g = gas

REFERENCES

1. Elmore, D. L., Robinson, W. W., and Watkins, W. B., "Dynamic Gas Temperature Measurement System," NASA CR-168267, Final Report for NASA Contract NAS3-23154. See also ISA Transactions 24, No. 2, pp. 73-82.

2. Dils, R. R., and Follansbee, P. S., "Wide Bandwidth Gas Temperature Measurements in Combustor and Combustor Exhaust Gases," Instrumentation in the Aerospace Industry, Vol. 22, Proceedings of the 22nd International Instrumentation Symposium, San Diego, Calif., 1976, pp. 307-328.

3. Yule, A. J., Taylor, D. S., and Chigier, B. A., "On-line Digital Compensation and Processing of Thermocouple Signals for Temperature Measurement in Turbulent Flames," AIAA 16th Aerospace Sciences Meeting, 16-18 January 1978, Paper No. 78-3.

4. Eckert, E. R. G., and Drake, R. M., Heat and Mass Transfer, 2nd Edition, 1959, McGraw-Hill, New York, p. 242.

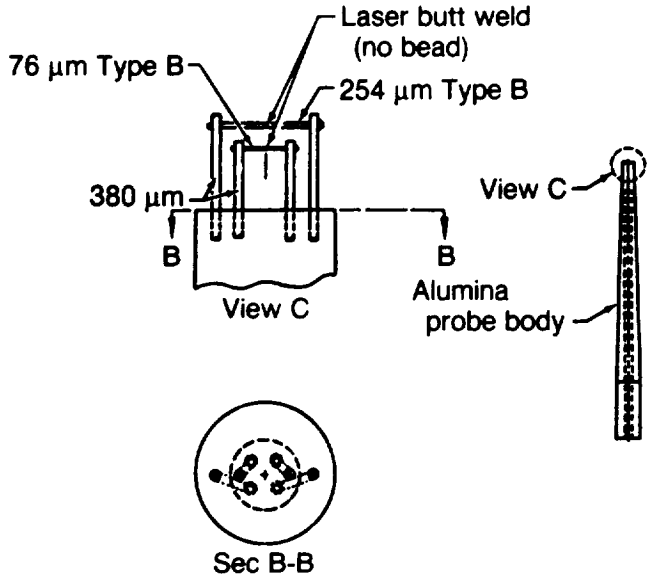

Fig. 1 Dynamic Temperature Sensor Concept

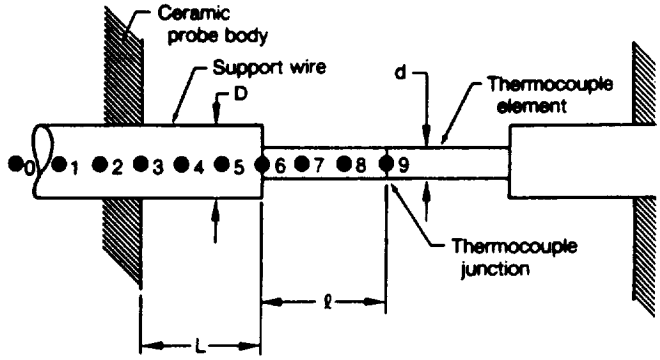

Fig. 2 Nine-Node Finite Difference Model

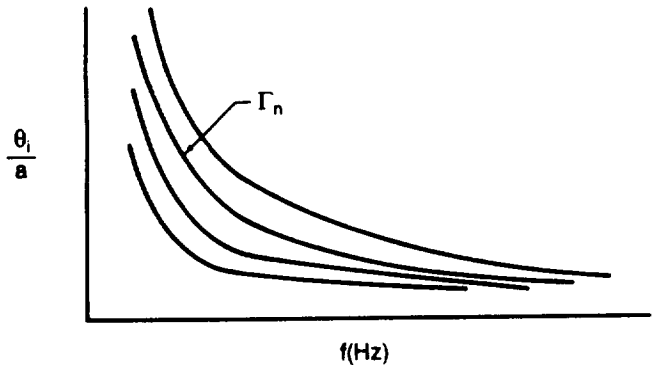

Fig. 3A Parametric Calculation Of θi(f)/a(f)

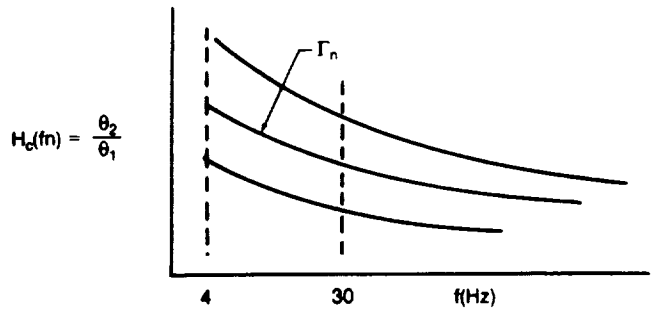

Fig. 3B Ratio θ_2/θ_1 For Several Values Of Γ

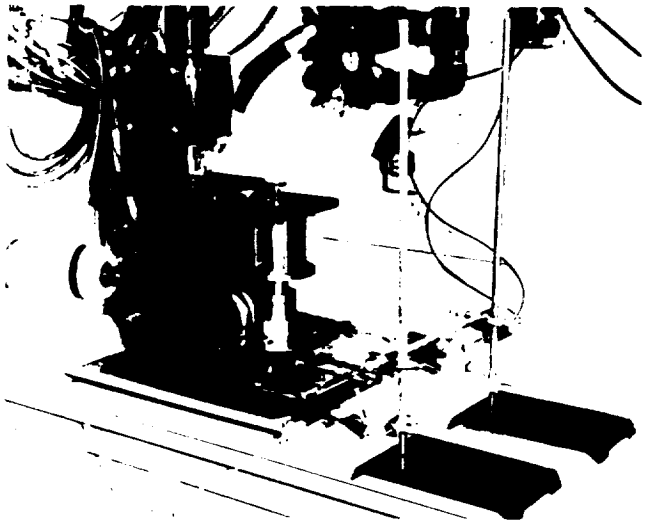

Fig. 4 Rotating Wheel Experiment θ

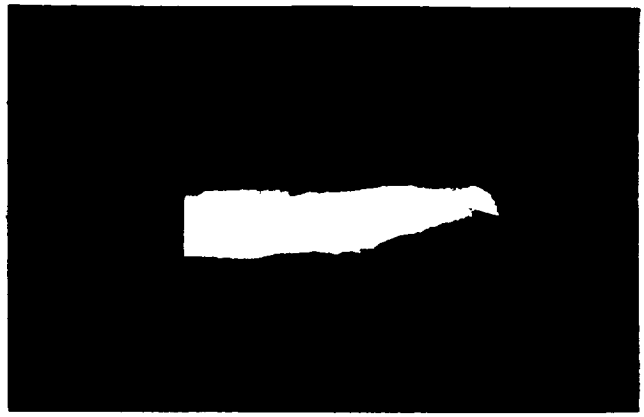

Fig. 5 Atmospheric Pressure Burner Experiment

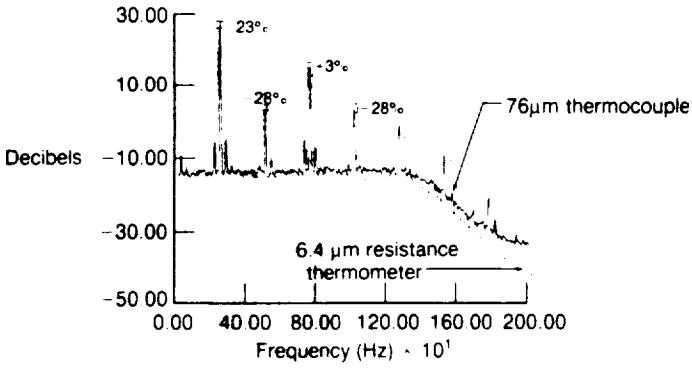

Fig. 6 Rotating Wheel Experiment Compensated 76μm And 6.4μm Sensor Power Spectral Densities

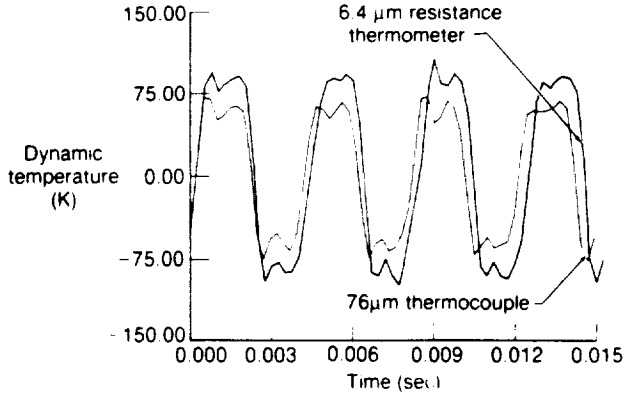

Fig. 7 Rotating Wheel Experiment Compensated 76μm And 6.4μm Sensor Wave-Forms

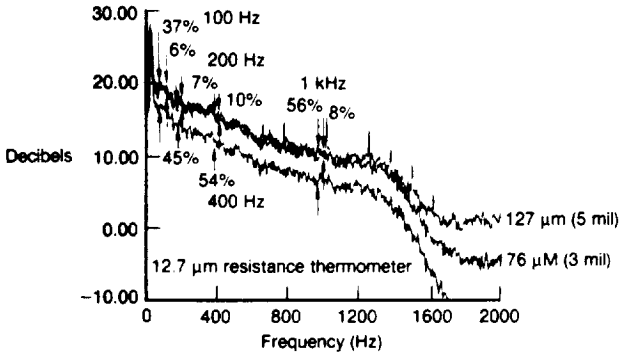

Fig. 8 Atmosphereric Pressure Burner Compensated Thermocouples And Resistance Thermometer Power Spectral Densities

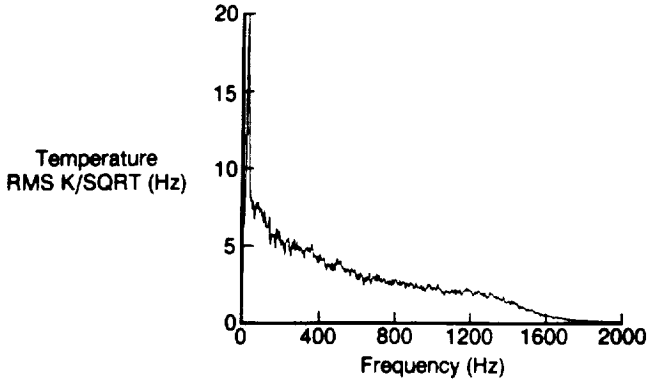

Fig. 9 Resistance Thermometer Linear Spectrum

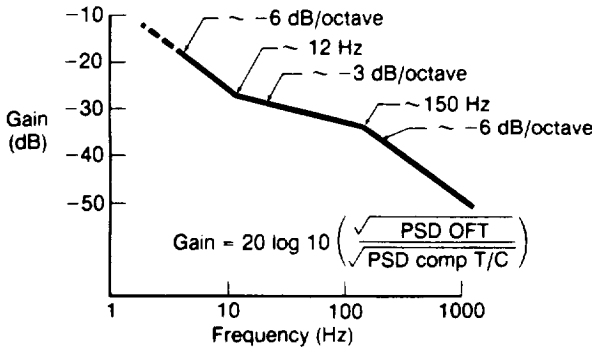

Fig. 10 Transfer Function Between Uncompensated Optical Fiber Thermometer And Compensated 76μm Thermocouple (1159K(1626°F) Test Point)

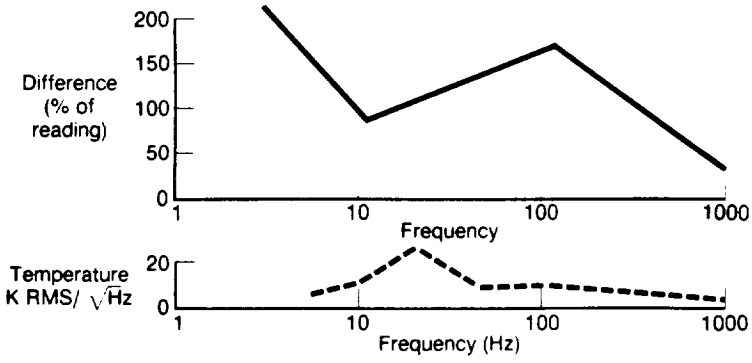

Fig. 11 Differences Between Optical Fiber Thermometer And 76μm Thermocouple Amplitudes (1159K (1626°F) Test Point)

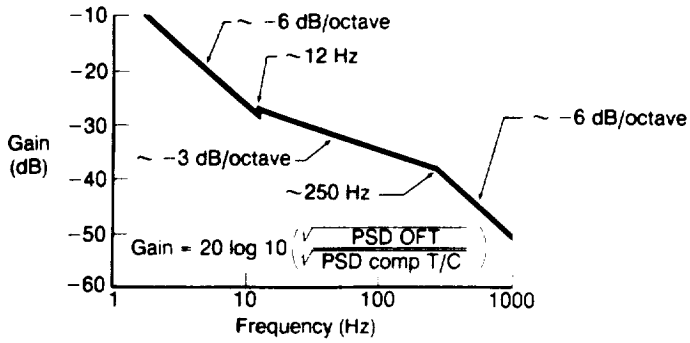

Fig. 12 Transfer Function Between Uncompensated Optical Fiber Thermometer and Compensated 76μm Thermocouple (1655K(2519°F) Test Point)

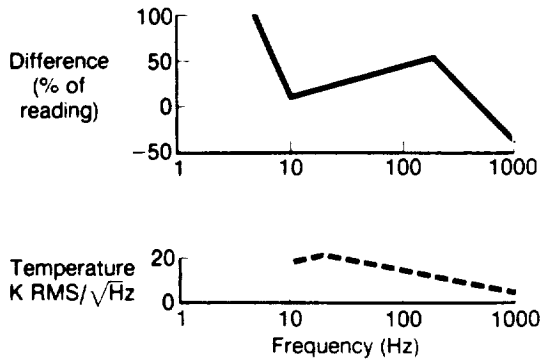

Fig. 13 Differences Between Optical Fiber Thermometer and 76μm Thermocouple Amplitudes (1655K(2519°F) Test Point)